

UNCLASSIFIED

Defense Technical Information Center
Compilation Part Notice

ADP012604

TITLE: A Bowtie Antenna Coupled Tunable Photon-Assisted Tunneling
Double Quantum Well [DQW] THz Detector

DISTRIBUTION: Approved for public release, distribution unlimited

This paper is part of the following report:

TITLE: Progress in Semiconductor Materials for Optoelectronic
Applications Symposium held in Boston, Massachusetts on November
26-29, 2001.

To order the complete compilation report, use: ADA405047

The component part is provided here to allow users access to individually authored sections
of proceedings, annals, symposia, etc. However, the component should be considered within
the context of the overall compilation report and not as a stand-alone technical report.

The following component part numbers comprise the compilation report:

ADP012585 thru ADP012685

UNCLASSIFIED

A Bowtie Antenna Coupled Tunable Photon-Assisted Tunneling Double Quantum Well (DQW) THz Detector

Majid M. Khodier¹, Christos G. Christodoulou¹, and Jerry A. Simmons²

¹The University of New Mexico

Dept. of Electrical & Computer Engineering

Albuquerque, NM 87131, U.S.A.

²Sandia National Laboratories

Albuquerque, NM 87185-1415, U.S.A.

ABSTRACT

The integration of a bowtie antenna with a double electron layer tunneling transistor (DELTT) device for the purposes of THz detection is investigated in this paper. The concept of THz detection, based on photon-assisted tunneling (PAT) between the two electron layers in a double quantum well (DQW) heterostructure, will be explained. The detector is expected to have narrowband, electrically tunable, fast response, and the possibility to operate at relatively high temperatures. Since the active area of the detector is very small, which is necessary to achieve fast response, it is not efficient in collecting THz radiation. Therefore, a broadband bowtie antenna is integrated with the detector to efficiently collect the THz radiation. Characteristics of different bowtie antenna geometries at THz frequencies were studied. An equivalent circuit model of the THz detector was developed, for the first time, to estimate the impedance characteristics at THz frequencies. Such a model is crucial for achieving impedance matching between the DELTT and the antenna to increase the overall coupling efficiency.

INTRODUCTION

The last frontier in high-frequency electronics research lies in the terahertz regime (other names are submillimeter wave or far infrared, FIR) between microwaves and the infrared (i.e., 0.3-15 THz). The technical advantages of the terahertz frequency regime are many (e.g., wider bandwidth, improved spatial resolution, compactness); however, the solid-state electronics capability within the THz frequency regime remains extremely limited from a basic signal source and systems perspective (i.e., output power < mwatts). This limited development results from the confluence of two fundamental factors. First, extremely challenging engineering problems exist in this region where wavelength is on the order of component size. Second, the practical and scientific applications of this shorter-wavelength microwave region have been restricted in the past to a few specialized fields (e.g., molecular spectroscopy). On the lower frequency side, electronic devices have an upper frequency limit of several hundred GHz due to transient times and parasitic RC time constants. On the higher frequency side, photonics devices, such as interband laser diodes, can only be operated at frequencies above the material's energy gap, which is greater than 40 meV (or 10 THz). Today, more and more important applications of THz technology are rapidly emerging that have civilian and military applications. For example, the strong absorption of electromagnetic energy

by atmospheric molecules, above 300 GHz, makes any communications link impossible to achieve. On the other hand, this same fundamental interaction mechanism suggests THz electronics to be a very promising tool for the identification and interrogation of chemical and biological (CB) agents. Other important applications of THz technologies, ranging from space exploration and atmospheric studies to plasma and fusion research, appear in [1]-[8].

In all of these applications, one kind of a detector or another is needed to transform the collected radiation into a useful electrical signal that can be related to the frequency and strength of that radiation. The THz detector discussed in this paper makes use of photon-assisted tunnelling (PAT) between multiple quantum wells (QWs) when the correct biasing is established, and the radiation has the correct frequency. A general characteristic of all detectors working at THz frequencies is the difficulty of coupling THz radiation efficiently to the active part of the detector for processing, and the prohibitive material losses at such high frequencies. The efficiency of the detector can be enhanced by incorporating an antenna, and since the first work at THz frequencies, it was realized that the antenna should be integrated lithographically with the detector, and the coupling of THz radiation should be done quasi-optically. The purpose of a feed antenna is to couple power from a wave in free space into a device that is much smaller than a wavelength. Since the performance of nearly all submillimeter and IR devices (diodes, tunnel junctions, etc) improves as their physical dimensions are reduced, feed antennas are a critical component of any system that transmits or receives high frequency radiation. Since high frequency devices are manufactured lithographically, it is natural to directly integrate the feed antenna onto the same dielectric substrate. The advantages of such lithographic antenna (or quasi-optical) are many. Compared to other feeding schemes such as waveguide coupling, the fabrication is much cheaper, more accurate, more robust, and more suitable for building large arrays. General reviews of lithographic antenna engineering for mm-wave and THz frequencies can be found in [9]-[15].

The principle of operation of the detector discussed in this paper is based on photon assisted tunnelling in a Double Electron Layer Tunnelling Transistor (DELTT). A general overview of the original structure of the detector is shown in Fig. 1. It consists of a bowtie antenna integrated with a DQW PAT THz detector. Since the detector area is very small, which is necessary for fast response, it cannot collect much of the THz radiation, and therefore, the detection of such radiation is very difficult. The bowtie antenna is used to efficiently collect the THz radiation and feed it to the detector for processing. Bowtie antenna is used because of its broadband response, easy design and fabrication, and its compatibility with the detector fabrication process. In the following sections, the principle of operation of the detector and its fabrication are briefly discussed. Then, simulation results of the bowtie antenna at THz frequencies are discussed. Finally, a simple and accurate equivalent circuit model of the THz detector is developed and discussed.

PRINCIPLE OF OPERATION

The basic idea is to bias the DELTT transistor so that it is off, i.e. tunnelling cannot occur because the dispersion curves of the two QWs do not coincide (the structure of the DELTT transistor is similar to that shown in Fig. 1, but without the bowtie antenna). An infrared photon of the correct energy can then be used to complete the energy-conservation conditions, adding energy to electrons in the higher density QW so that they can resonantly

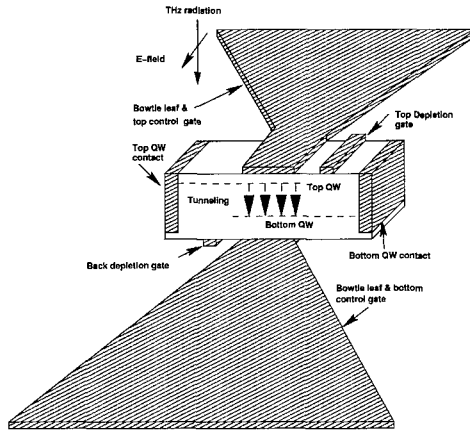


Figure 1: An overview of the DQW THz detector integrated with a bowtie antenna. The top and bottom bows are connected to the top and bottom control gates, respectively. The control gates are used to change the density of electrons in each QW, and therefore provide the electrical tunable characteristic through a DC bias. The depletion gates are used to deplete the QW the one does not wish to contact. The top QW contact is called the source, and the bottom QW contact is called the drain. The structure without the bowtie antenna is called DELTT.

tunnel into the lower density QW. Conceptually, the device behaves analogously to a p-n junction photodiode: in order for electrons to move from the high potential region to the low potential region, they must first overcome an energy barrier. In the p-n junction photodiode, this is accomplished by exciting an electron from the valence band to the conduction band, i.e. creating an electron-hole pair. In the DELTT THz detector, however, this is accomplished by exciting an electron at a given transverse momentum in one QW, to a higher energy state at the same \mathbf{k} in the other QW, as shown in Fig. 2. In the absence of photons, resonant tunnelling can only occur when there exist states in both QWs with identical energy and in-plane momentum. Because both layers are 2D, their allowed states each form a paraboloid having states only on the surface. Without THz radiation, no pairs of states of identical momentum and energy exist, and so tunnelling does not occur. A THz photon of the correct energy, however, will complete the energy-conservation conditions by exciting an electron at a given in-plane momentum \mathbf{k} in one QW, to a higher energy state at the same \mathbf{k} in the other QW. This photon-assisted tunnelling transition causes current to flow between source and drain. What is unique and exciting about the DQW photodetector is that (1) neglecting higher subbands, only a single energy will complete the energy conservation conditions for all the electrons, irrespective of their in-plane momentum values \mathbf{k} , and this results in a very narrowband response. In addition, (2) the energy of the transition can be readily controlled by a gate voltage and/or source drain bias V_{SD} , which makes it possible to obtain a tunable THz detector. A more detailed discussion about the device operation and fabrication can be found in [16]-[21].

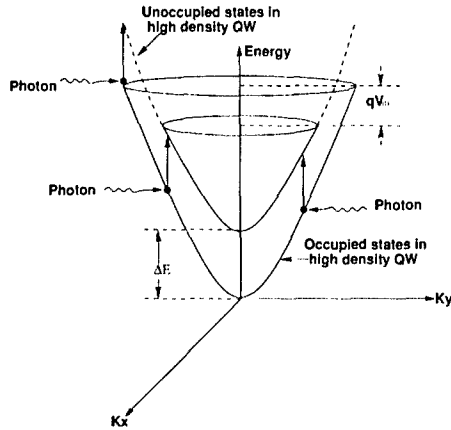


Figure 2: Sketch of the dispersion curve of a double quantum well FIR detector structure.

By applying DC bias to the top or bottom control gate, the electron density in either QW will change accordingly, and the peak of the tunneling current will change in position and magnitude. Therefore, the control gates can be used to create an electrically tunable THz detector over a broadband of THz frequencies.

The DQW structure is an MBE-grown modulation doped heterostructure using the $\text{Al}_x\text{Ga}_{1-x}\text{As}$ material system. Then, the EBASE technique [21] is used to finish the fabricate of the DQW structure by adding front and back gates. Here, we briefly discuss the basic steps involved in the device fabrication as shown in Figure 3, and a more detailed discussion about the fabrication process is found in [21]. The first step is to grow the double quantum well epitaxial structure on a sacrificial substrate. Then, the front side of the structure is processed by making the ohmic contacts and patterning the top gates using conventional methods, as shown in Figure 3(a). After processing the front side, the sample is epoxied to a host substrate as shown in Figure 3(b). Then, the original sacrificial substrate on which the active layers were grown is removed by etching as shown in Figure 3(c). Etching stops on a $\text{Al}_{0.72}\text{Ga}_{0.28}\text{As}$ stop etch layer grown at the base of the epitaxial layer structure. Finally, the back surface is processed by patterning the back gates and etching via holes through the active layers to the front side electrical contact pads for the gates and ohmic contacts as shown in Figure 3(d).

The different dielectric and metallic layers that are used to construct the detector are shown in Fig. 4. The active area of the detector is about $10\mu\text{m} \times 12\mu\text{m}$, which is only a small fraction of the whole detector area (including the antenna). The most important layers in Fig. 4 are the active layer which contains the QWs, the epoxy layer, and the GaAs substrate. The leaves of a bowtie antenna are connected to the top and bottom control gates, as shown in Fig. 1. A photo of a THz DQW detector with bowtie antenna fabricated at Sandia National Laboratory is shown in Fig. 5.

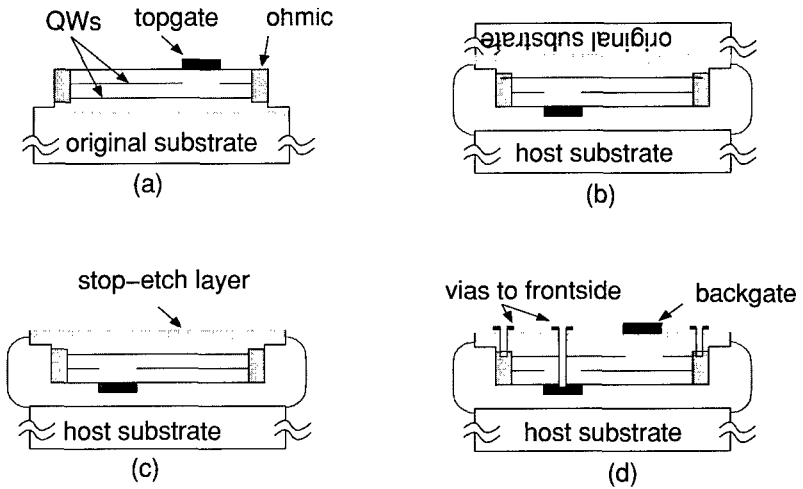


Figure 3: Main steps in the device fabrication using the EBASE technique (a) pattern frontside, (b) epoxy frontside down to host substrate, (b) remove original substrate by etching to stop-etch layer, and (d) pattern backside, including backgates and vias to frontside electrical contact pads.

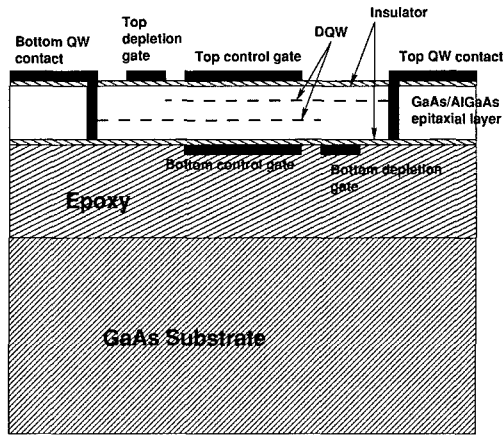


Figure 4: Cross sectional view of the DQW THz detector showing the different dielectric and metallic layers used in the device after fabrication. The GaAs substrate thickness is about $500 \mu\text{m}$, epoxy layer of about $2 \mu\text{m}$, and the epitaxial layer of about $1 \mu\text{m}$. The insulator thickness is about 200 \AA .

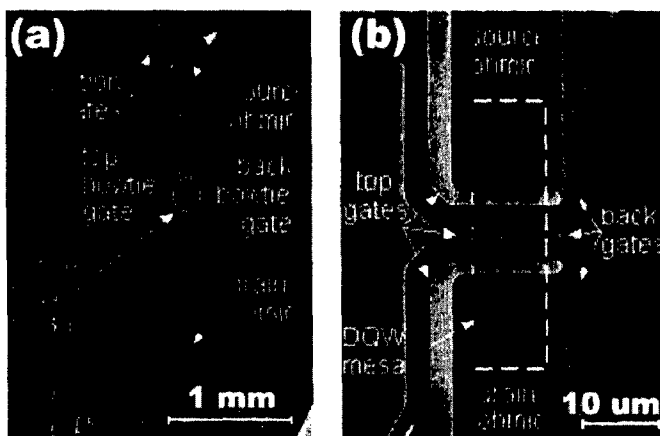


Figure 5: (a) An SEM photo of a bowtie antenna fabricated with the DQW PAT THz detector. The photo corresponds to the design shown schematically in Fig. 1, and (b) Zoomed-in view of (a), showing the active DQW mesa. The bottom gates, although beneath the semiconductor epitaxial layers, remain visible since the electron beam easily penetrates them.

BOWTIE ANTENNA SIMULATION

When the bowtie antenna shown in Fig. 5, which has a bow angle of 120° , is simulated, the results showed that the antenna does not have a broadband characteristic around the frequency of interest (2.54 THz). A new bowtie antenna layout is proposed as shown in Fig. 6(a). This antenna has a bow angle of 90° which gives a self complementary design, and therefore has a theoretical constant real input impedance equals to $60\pi \Omega$ when the antenna is suspended in free space [15]. The purpose of this antenna is to serve as a broadband antenna for coupling the THz radiation to the DQW detector. The antenna structure is simulated on top of a $500 \mu\text{m}$ GaAs substrate using the IE3D simulator [22]. The total length of the antenna is $80 \mu\text{m}$. The antenna length is chosen to be approximately two wavelengths long at 2.54 THz when the antenna is placed on top of a GaAs substrate of $\epsilon_r = 13.1$. The free space wavelength at 2.54 THz is approximately $120 \mu\text{m}$, and assuming an effective dielectric constant of 9, then the wavelength of the combined free space and substrate structure is about $40 \mu\text{m}$. The simulated values of the input impedance is shown in Fig. 6(b). The value of the real part is about 75Ω , and the magnitude of the imaginary part less than 20Ω . The theoretical value the input impedance of a self complementary antenna on a GaAs substrate is real and equals approximately to 74Ω , which is very close from the value obtained from the simulation results.

CIRCUIT MODEL

In order to achieve maximum coupling between the device and the incoming beam, the

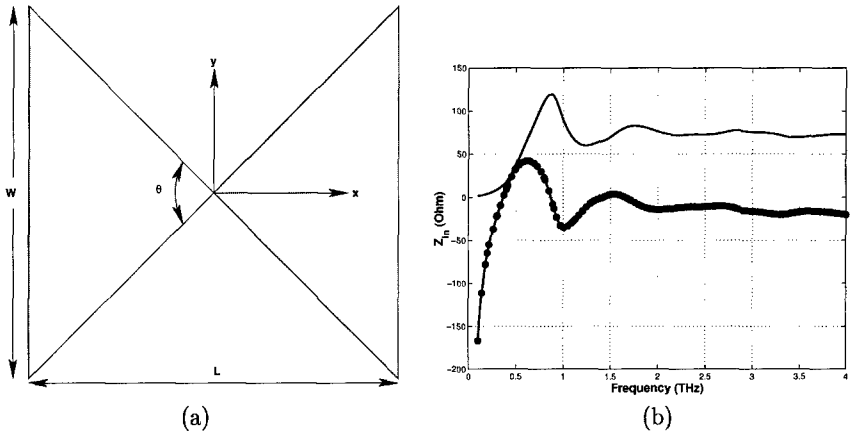


Figure 6: (a) Layout of the 90° bowtie antenna. (b) Input impedance vs. frequency. Solid line: real part, line with dots: imaginary part.

device impedance should be equal to the complex conjugate of the antenna impedance. For this purpose, a method to estimate the frequency dependent impedance of the DELTT is required. This can be achieved by developing an equivalent circuit model of the device which incorporates all the important physical processes and geometrical dimensions that affect the device operation.

A lumped circuit model for the DELTT, valid at DC, is presented in [23]. Another equivalent circuit model for a single two-dimensional electron gas (2DEG) which is capacitively contacted to metallic gates was presented in [24], based on the concept of kinetic inductance. The circuit model consists of either lumped elements or distributed elements (i.e. transmission line), depending on the structure dimensions. The validity of the model at microwave frequencies was also experimentally verified in [24]. In [25], an equivalent model for a DQW was developed using transmission line theory. However, the model did not take into consideration the presence of a gate on top or below (or both) of the DQW structure. The subject of this paper is to develop a general equivalent circuit model for the DELTT structure, which has both top and bottom gates. This work represents an extension to the work found in [24] and [25] to include the effect of the top and bottom gates.

The Drude model for the frequency dependent resistivity of a single 2DEG layer is [24]:

$$\rho(\omega) = \frac{m^*}{ne^2\tau_{mom}} (1 + j\omega\tau_{mom}) \quad (1)$$

where n is the electron density, e the electron charge, m^* the effective mass, and τ_{mom} the momentum scattering time. Equation 1 is the sum of a real part, which is the resistance, and a positive, frequency dependent, imaginary part, which can be considered as an inductive reactance. This inductance is known as the kinetic inductance, because the inductive energy is stored in the kinetic energy of the electrons. At low frequencies, the imaginary part of ρ is very small and usually neglected when developing circuit models for the 2DEG. At THz

frequencies, however, the imaginary part becomes dominant, and it is necessary to include in any circuit model. It should be mentioned that the momentum scattering time τ_{mom} in modulation doped MBE-grown, high mobility GaAs/AlGaAs structures at low temperatures ($< 4K$) is 3-4 orders of magnitude larger than in conventional, bulk doped semiconductors at room temperature.

To ease the calculation of the equivalent circuit model for the DELTT, its cross section is divided into three different regions, as shown in Figure 7. These regions are:

- Region 1: this region consists of a section of either the top or the bottom QW, and extends from the source (or drain) contact to the end of the bottom (or top) depletion gate. In this region, there is no tunneling. The equivalent circuit for this region is composed basically of a resistance in series with inductance. The length of this regions is L_1 .
- Region 2: this region consists of the section of the DELTT between the control gates and the depletions gates where there is overlap between the top and the bottom QWs, and in this region tunneling can occur. The equivalent circuit for this region is a transmission line of length L_2 . An incremental length of this region consists of a resistance R in series with an inductance L , to model each QW, and a shunt capacitance C and conductance G to model the capacitance and the tunneling conductance between the top and bottom QWs. The values of the elements in this region are per unit length.
- Region 3: this region consists of the section of the DELTT where there is overlap between the top and bottom QWs, and covered by the top and bottom control gates, and in this region tunneling can occur. The equivalent circuit for this region is also a transmission line of length L_3 . An incremental length of this region has a similar circuit as that of region 2, but with an extra top and bottom capacitors, C_t and C_b , to model the contact capacitances between the top control gate and top QW, and between the bottom control gate and bottom QW, respectively. The values of the elements in this region are per unit length.

It should be mentioned that the DELTT structure studied here is symmetrical, i.e. electron densities in both QWs are the same. The overall equivalent circuit model for the DELTT transistor, with an antenna connected between the top and bottom control gates, is shown in Figure 8. In terms of mobility μ , surface density n , the width w , dielectric permittivity ϵ of the material between the QWs, and distance between the two QWs d_{qw} , the values of R , L , and C in Figure 8 are given by:

$$R = \frac{1}{en\mu w} \quad (2)$$

$$L = \frac{m^*}{e^2 n w} \quad (3)$$

$$C = \epsilon \times \frac{d_{qw}}{w} \quad (4)$$

The small signal tunneling conductance G can be obtained from the I-V curve of the DELTT by taking the derivative of the current with respect to the applied bias. The element values,

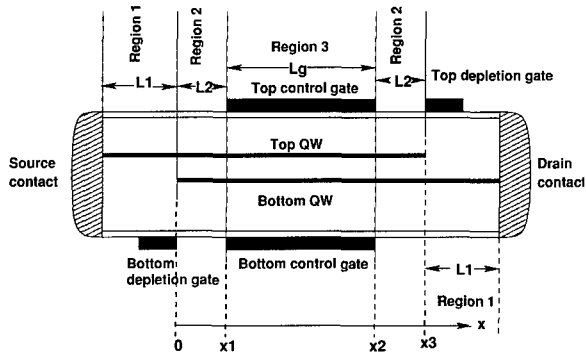


Figure 7: Cross section of the DELTT showing the three regions used in the calculation of the equivalent circuit.

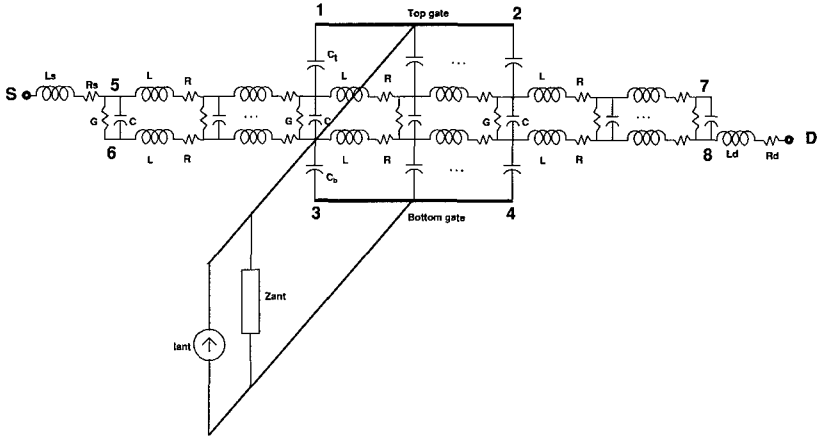


Figure 8: Equivalent circuit model of the DELTT with an antenna connected between the top and bottom control gates. The antenna is modelled as a current source in parallel with the antenna impedance.

R_s , L_s , R_d , and L_d , shown in Figure 8 can be calculated from equations 2 and 3 by multiplying the result from each equation by the length L_1 . The remaining elements, C_t and C_b , represent the geometrical capacitance between the top gate and the top QW and that between the bottom gate and bottom QW, respectively, and can be calculated as follows:

$$C_t = \epsilon \times \frac{d_t}{w} \quad (5)$$

$$C_b = \epsilon \times \frac{d_b}{w} \quad (6)$$

where d_t and d_b are the distances between the top gate and the top QW, and the bottom gate

and bottom QW, respectively, and ϵ is the dielectric permittivity of the material between each gate and the corresponding QW.

We can analyze the structure shown in Fig. 8 by assigning position dependent voltage and current for each transmission line, and then solve the resulting coupled differential equations. The result will be the position dependent voltage and current for each line. The input impedance between any two points in Fig. 8 can be found by applying the appropriate boundary conditions and solving for the unknown coefficients, and then divide the appropriate voltage and current. The details of the analysis can be found in [26]. In the following subsections, the input impedance of the DELTT between the source (S) and the Drain (D), and between the top and bottom control will be calculated using the equivalent circuit shown in Fig. 8. These are the two possible locations where an antenna can be connected to the DELTT device. Sample parameters values for a DELTT device (Sample G1717) will be used in the calculations, and these parameters are shown Table 1.

Table 1: Sample parameters for the DELTT sample G1717. The listed parameters are QW widths (w_{qw}), tunnel barrier thickness (d_{qw}), electron densities for the top and bottom QWs (n_t and n_b measured in 10^{11}cm^{-2}), distance from top control gate to top QW (d_t) and distance from bottom control gate to bottom QW (d_b), device channel width (w_{chan}), length of the control gates (L_{cg}), length of the depletion gates (L_{dg}), and the separation between the control gates and depletion gates (L_{cg-dg}).

Sample	w_{qw} (Å)	d_{qw} (Å)	n_t	n_b	d_t (μm)	d_b (μm)	w_{chan} (μm)	L_{cg} (μm)	L_{dg} (μm)	L_{cg-dg} (μm)
G1717	150	125	2.0	1.4	0.13	2.2	500	40	10	5

Calculating Z_{SD}

To calculate the input impedance between the source and the drain, Z_{SD} , the equations of the voltages and currents in the three regions are solved for the unknown coefficients using the boundary conditions of a voltage source at point S , and a ground at the drain, D . After finding the unknown coefficients, the input current at the source is found, and then the voltage is divided by the current at the source to obtain Z_{SD} . Element values like R , L , C , C_t , C_b , R_s , R_d , L_s , and L_d are calculated from the parameters in Table 1 using equations 2-6. Applying the above procedure, we calculated Z_{SD} as a function of frequency and the result is shown in Fig. 9(b). The imaginary part of Z_{SD} increases slowly with frequency because of the source and drain conductances (L_s and L_d). The results show that the high frequency limit is basically that of an inductor. Each extra peak with increasing frequency corresponds to fitting one more wavelength into the combined length of regions 2 and 3.

Calculating Z_{13}

The impedance Z_{13} represents the impedance of the DELTT between the top and the bottom control gates where an antenna can be connected. This impedance can be calculated

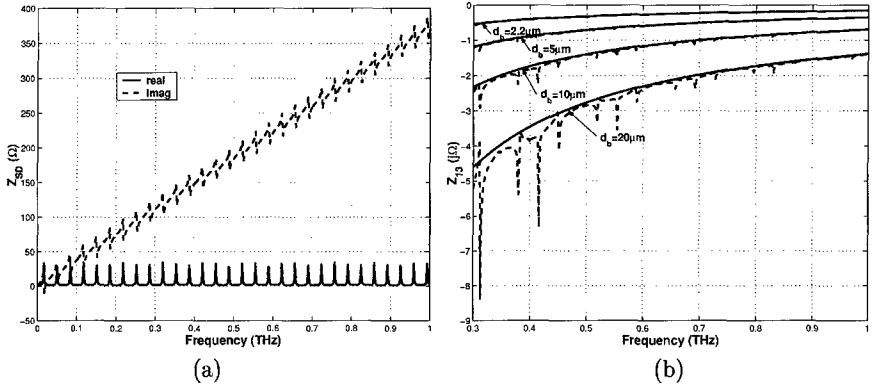


Figure 9: (a) Simulation results of Z_{SD} for the G1717 sample. (b) Simulation (solid line) and predicted (dashed line) results of Z_{13} for the G1717 sample at different values of d_b .

by applying a voltage source at point 1, grounding points 3, S, and D in Figure 8, solving the equations of the voltages and currents in the three regions for the unknown coefficients, and then dividing the voltage by the current at point 1. Simulation results for the G1717 sample are shown in Fig. 9(b) for different values of d_b . The input impedance Z_{13} has a very small real part (negligible and not shown in the figure), and a negative imaginary part that resembles the reactance of a capacitor. We propose that Z_{13} is simply the series combination of Y_t , Y , and Y_b , and therefore Z_{13} is given by:

$$Z_{13} = \frac{1}{L_{cg}} \left(\frac{1}{Y} + \frac{1}{Y_t} + \frac{1}{Y_b} \right) \quad (7)$$

where $Y = G + j\omega C$, $Y_t = j\omega C_t$, $Y_b = j\omega C_b$, and L_{cg} is the length of the control gate(s). We calculated Z_{13} using equation 7 and the results are shown in Fig. 9(b) for different values of d_b . The simulation results and the theoretical results shown in Fig. 9(b) agree very well, which suggests that equation 7 is accurate enough to predict Z_{13} of the DELTT structure.

CONCLUSIONS

The potential of THz detection based on the idea of photon-assisted tunneling in double quantum well devices was introduced. The basic principle of operation of the detector was discussed, and the detector fabrication using state-of-the-art techniques were also presented in this paper. The necessity of integrating a broadband antenna with the device was also established. Simulation results show that it is possible to achieve broadband antenna using self complementary design. This paper also presented for the first time a general equivalent circuit model for the DELTT device. Measurements at very high frequencies can be very difficult to obtain since it is extremely difficult to obtain accurate measurements of impedance at such high frequencies. However, the presented circuit model, based on the most important physical interactions that affect the device operation, can be utilized at THz frequencies,

assuming that the device parameters (like density and mobility) at these high frequencies can be determined accurately. Moreover, the simulations results of sample devices revealed that it is extremely difficult to match the DELTT impedance to the broadband band bowtie antenna impedance.

REFERENCES

- [1] J. W. Waters and P. H. Siegel, "Applications of Millimeter and Submillimeter Technology to Earth's Upper Atmosphere: Results to Date and Potential for the Future," *The 4th International Symposium on Space Terahertz Technology*, Los Angeles, CA, March 1993.
- [2] J. Farman, B. Gardiner, and J. Shanklin, "Large Losses of Total Ozone in Antarctica Reveal seasonal ClO_x/NO_x ," *Nature*, Vol. 315, p. 207, 1985.
- [3] P. B. Hays and H. E. Snell, "Atmospheric Remote Sensing in the Terahertz Regions," *Proceedings of the 1st International Symposium on Space Terahertz Technology*, p. 482, 1990.
- [4] T. G. Phillips, "Developments in Submillimeter-Wave Astronomy," *The 19th International Conference on Infrared and Millimeter Waves*, Sendai, Japan, 1994.
- [5] S. Gulkis, "Submillimeter Wavelength Astronomy Missions for the 1990s," *Proceedings of the 1st International Symposium on Space Terahertz Technology*, pp. 454-457, 1990.
- [6] N. C. Luhmann, "Instrumentation and Techniques for Plasma Diagnostics: An Overview," *Infrared and Millimeter Waves*, Vol. 2, pp. 1-65, K. J. Button, Ed., Academic Press, New York, 1979.
- [7] P. E. Young, D. F. Neikirk, P. P. Tong, and N. C. Luhmann, "Multi-channel Far-infrared Phase Imaging for Fusion Plasma," *Rev. Sci. Instrum.*, Vol. 56, pp. 81-89, 1985.
- [8] P. F. Goldsmith, "Coherent Systems in the Terahertz Frequency Range: Elements, Operation and Examples," *Proceedings of the 3rd International Symposium on Space Terahertz Technology*, pp. 1-23, 1992.
- [9] R. A. York and Z. B. Popovic, Ed., *Active and Quasi-Optical Arrays for Solid-State Power Combining*, John wiles & Sons, New York, 1997.
- [10] D. B. Rutledge, D. P. Neikirk, and D. P. Kasilingham, "Integrated-Circuit Antennas," *Infrared and Millimeter Waves*, Vol. 10, New York, Academic Press, 1983, ch. 1, pp. 1-90.
- [11] M. Rebiez, "Millimeter-Wave and Terahertz Integrated Circuit Antennas," *Proc. Of the IEEE*, Vol. 80, pp. 1748-1770, Nov. 1992.
- [12] E. N. Grossman, "Lithographic Antennas for Submillimeter and Infrared Frequencies," *IEEE International Symposium on Electromagnetic Compatibility*, pp. 102-107, 1995

- [13] D. S. Hernandez and I. Robertson, "Integrated Antennas for TeraHertz Circuits," *IEEE Colloquium on Terahertz Technology*, pp. 1-7, 1995.
- [14] D. B. Rutledge, S. E. Schwarz and A. T. Adams, "Infrared and Submillimeter Antennas," *Infrared Physics*, Vol. 18, pp. 713-729, Pergamon Press Ltd, 1978.
- [15] R. C. Compton et al, "Bow-Tie Antennas on a Dielectric Half-Space: Theory and Experiment," *IEEE Trans. Antennas Propagat.*, Vol. 35, pp. 622-630, June 1987.
- [16] Sanchez, C. F. Davis, K. C. Liu and A. Javan, "The MOM Tunneling Diode: Theoretical Estimate of its Performance at Microwave and Infrared Frequencies," *J. Appl. Phys.*, Vol. 49(10), pp. 5270-5277, Oct. 1978.
- [17] H. Drexler, J. S. Scott and S. J. Allen, "Photon-Assisted Tunneling in a Resonant Tunneling Diode: Stimulated Emission and Absorption in the THz Range," *Appl. Phys. Lett.*, Vol. 67(19), pp. 2816-2818, Nov. 1995.
- [18] J. A. Simmons et al, "Planar Quantum Transistor Based on 2D-2D Tunneling in Double Quantum Well Heterostructure," *J. Appl. Phys.*, Vol. 84(10), pp. 5626-5634, Nov. 1998.
- [19] M. A. Blout et al, "Double Electron Layer Tunneling Transistor (DELTT)," *Semicond. Sci. Technol.*, Vol. 13, pp. A180-A183, 1998.
- [20] J. S. Moon et al, "Unipolar Complementary Circuits Using Double Electron Layer Tunneling Transistor," *Appl. Phys. Lett.*, Vol. 74, pp. 314-316, Jan. 1999.
- [21] M. V. Weckwerth et al, "Epoxy Bond and Stop-Etch (EBASE) Technique Enabling Backside Processing of (Al)GaAs Heterostructures," *Superlattices and Microstructures*, Vol. 20, No. 4, pp. 561-567, 1996.
- [22] IE3D is a Registered Trademark of Zeland Software, Inc.
- [23] Y. Katayama and D. C. Tsui, "Lumped Circuit Model of Two-Dimensional to Two-Dimensional Tunneling Transistors," *Appl. Phys. Lett.*, Vol. 62 (20), pp. 2563-2565, May 1993.
- [24] P. J. Burke, I. B. Spielman and J. P. Eisenstein, "High Frequency Conductivity of the High-Mobility Two-Dimensional Electron Gas," *Appl. Phys. Lett.*, Vol. 76, pp. 745-747, Feb. 2000.
- [25] P. J. Burke and J. P. Eisenstein, "Interlayer Plasmons," *unpublished report*, August 1998.
- [26] M. M. Khodier, *Analysis and Design of Broadband Antennas for the Double Quantum Well Terahertz Detector*, Ph.D. dissertation, The University of New Mexico, Albuquerque, NM, 2001.